Title
Femtosecond laser-matter interactions in ternary zinc phosphate glasses

Journal
Optical Materials Express, 8(12)

ISSN
2159-3930

Authors
Hernandez-Rueda, J
Troy, NW
Freudenberger, P
et al.

Publication Date
2018-12-01

DOI
10.1364/ome.8.003622

Peer reviewed

Femtosecond Laser-Matter Interactions in Ternary Zinc Phosphate Glasses

Javier Hernandez-Rueda,[1,2,*] **Neil W. Troy,**[1] **Parker Freudenberger,**[3] **Richard K. Brow,**[3] **and Denise M. Krol**[1]

[1] *Department of Materials Science and Engineering, University of California Davis, California 95616, USA*
[2] *Debye Institute for Nanomaterials Science, Utrecht University, P.O. Box 80000, 3508 TA Utrecht, The Netherlands*
[3] *Missouri University of Science and Technology, Rolla, MO 65409, USA*
[*] *fjavihr@gmail.com*

Abstract: We investigate the interaction of ultrashort laser pulses with ternary zinc phosphate glasses. We explore the viability of ten different glass compositions with different levels of alumina to inscribe optical waveguides via fs-laser direct writing technique, finding that only samples with [O]/[P] ratios of 3.25 are suitable candidates. We also test a zinc magnesium phosphate glass to fabricate waveguide Bragg gratings in order to generate filters and mirrors with specific spectral properties. Confocal Raman spectroscopy inspection shows that laser-damaged material exhibits a relative intensity decrease and a subtle blue-shift on the 1209 cm^{-1} Raman peak, which implies a relative reduction on the content of $Q^{(2)}$ tetrahedra species within the glass network thus suggesting a laser-induced depolymerization. In contrast, optical waveguides and smooth laser-induced changes do not exhibit such noticeable structural modifications.

OCIS codes: (000.0000) General; (000.2700) General science.

References and links

1. Christian Wagner and Noreen Harned. Euv lithography: Lithography gets extreme. *Nature Photonics*, 4(1):24, 2010.
2. Alfred Vogel and Vasan Venugopalan. Mechanisms of pulsed laser ablation of biological tissues. *Chemical Reviews*, 103(2):577–644, 2003. PMID: 12580643.
3. Rafael R. Gattass and Eric Mazur. Femtosecond laser micromachining in transparent materials. *Nature Photonics*, 2:219, April 2008.
4. Eli N Glezer and Eric Mazur. Ultrafast-laser driven micro-explosions in transparent materials. *Applied physics letters*, 71(7):882–884, 1997.
5. C Hnatovsky, RS Taylor, E Simova, PP Rajeev, DM Rayner, VR Bhardwaj, and PB Corkum. Fabrication of microchannels in glass using focused femtosecond laser radiation and selective chemical etching. *Applied Physics A*, 84(1-2):47–61, 2006.
6. Chris B Schaffer, Andre Brodeur, and Eric Mazur. Laser-induced breakdown and damage in bulk transparent materials induced by tightly focused femtosecond laser pulses. *Measurement Science and Technology*, 12(11):1784, 2001.
7. Graham D Marshall, Alberto Politi, Jonathan CF Matthews, Peter Dekker, Martin Ams, Michael J Withford, and Jeremy L OâĂŹBrien. Laser written waveguide photonic quantum circuits. *Optics express*, 17(15):12546–12554, 2009.
8. S Taccheo, G Della Valle, R Osellame, G Cerullo, N Chiodo, P Laporta, O Svelto, Alexander Killi, Uwe Morgner, Max Lederer, et al. Er: Yb-doped waveguide laser fabricated by femtosecond laser pulses. *Optics letters*, 29(22):2626–2628, 2004.
9. Quan Sun, Hongbing Jiang, Yi Liu, Yongheng Zhou, Hong Yang, and Qihuang Gong. Effect of spherical aberration on the propagation of a tightly focused femtosecond laser pulse inside fused silica. *Journal of Optics A: Pure and Applied Optics*, 7(11):655, 2005.
10. A Marcinkevičius, Vygantas Mizeikis, S Juodkazis, S Matsuo, and Hiroaki Misawa. Effect of refractive index-mismatch on laser microfabrication in silica glass. *Applied Physics A*, 76(2):257–260, 2003.
11. K Miura Davis, Kiyotaka Miura, Naoki Sugimoto, and Kazuyuki Hirao. Writing waveguides in glass with a femtosecond laser. *Optics letters*, 21(21):1729–1731, 1996.
12. K Miura, Jianrong Qiu, H Inouye, T Mitsuyu, and K Hirao. Photowritten optical waveguides in various glasses with ultrashort pulse laser. *Applied Physics Letters*, 71(23):3329–3331, 1997.
13. K Hirao and K Miura. Writing waveguides and gratings in silica and related materials by a femtosecond laser. *Journal of non-crystalline solids*, 239(1-3):91–95, 1998.

14. ND Psaila, RR Thomson, HT Bookey, AK Kar, N Chiodo, R Osellame, G Cerullo, A Jha, and S Shen. Er: Yb-doped oxyfluoride silicate glass waveguide amplifier fabricated using femtosecond laser inscription. *Applied Physics Letters*, 90(13):131102, 2007.
15. Alexander M Streltsov and Nicholas F Borrelli. Study of femtosecond-laser-written waveguides in glasses. *JOSA B*, 19(10):2496–2504, 2002.
16. Javier Hernandez-Rueda, Jasper Clarijs, Dries van Oosten, and Denise M Krol. The influence of femtosecond laser wavelength on waveguide fabrication inside fused silica. *Applied Physics Letters*, 110(16):161109, 2017.
17. Jon J Witcher, Javier Hernandez-Rueda, and Denise M Krol. Fs-laser processing of glass: Plasma dynamics and spectroscopy. *International Journal of Applied Glass Science*, 6(3):220–228, 2015.
18. PS Salter, Alexander Jesacher, JB Spring, BJ Metcalf, N Thomas-Peter, Richard D Simmonds, NK Langford, IA Walmsley, and Martin J Booth. Adaptive slit beam shaping for direct laser written waveguides. *Optics letters*, 37(4):470–472, 2012.
19. L Englert, B Rethfeld, L Haag, M Wollenhaupt, Cristian Sarpe-Tudoran, and T Baumert. Control of ionization processes in high band gap materials via tailored femtosecond pulses. *Optics Express*, 15(26):17855–17862, 2007.
20. Javier Hernandez-Rueda, Jan Siegel, Marcial Galvan-Sosa, Alexandro Ruiz de la Cruz, and Javier Solis. Surface structuring of fused silica with asymmetric femtosecond laser pulse bursts. *JOSA B*, 30(5):1352–1356, 2013.
21. James W Chan, Thomas R Huser, Subhash H Risbud, Joseph S Hayden, and Denise M Krol. Waveguide fabrication in phosphate glasses using femtosecond laser pulses. *Applied physics letters*, 82(15):2371–2373, 2003.
22. Luke B Fletcher, Jon J Witcher, Neil Troy, Signo T Reis, Richard K Brow, and Denise M Krol. Direct femtosecond laser waveguide writing inside zinc phosphate glass. *Optics express*, 19(9):7929–7936, 2011.
23. Luke B Fletcher, Jonathan J Witcher, Neil Troy, Signo T Reis, Richard K Brow, Rebeca Martinez Vazquez, Roberto Osellame, and Denise M Krol. Femtosecond laser writing of waveguides in zinc phosphate glasses. *Optical Materials Express*, 1(5):845–855, 2011.
24. Luke B Fletcher, Jon J Witcher, Neil Troy, Signo T Reis, Richard K Brow, and Denise M Krol. Effects of rare-earth doping on femtosecond laser waveguide writing in zinc polyphosphate glass. *Journal of applied physics*, 112(2):023109, 2012.
25. Luke B Fletcher, Jon J Witcher, Neil Troy, Richard K Brow, and Denise M Krol. Single-pass waveguide amplifiers in er-yb doped zinc polyphosphate glass fabricated with femtosecond laser pulses. *Optics letters*, 37(7):1148–1150, 2012.
26. Martin Ams, GD Marshall, DJ Spence, and MJ Withford. Slit beam shaping method for femtosecond laser direct-write fabrication of symmetric waveguides in bulk glasses. *Optics express*, 13(15):5676–5681, 2005.
27. Graham D Marshall, Martin Ams, and Michael J Withford. Direct laser written waveguide-bragg gratings in bulk fused silica. *Optics Letters*, 31(18):2690–2691, 2006.
28. J Hernandez-Rueda, D Puerto, J Siegel, M Galvan-Sosa, and J Solis. Plasma dynamics and structural modifications induced by femtosecond laser pulses in quartz. *Applied Surface Science*, 258(23):9389–9393, 2012.
29. Javier Hernandez-Rueda, Nadine GoÌĹtte, Jan Siegel, Michelina Soccio, Bastian Zielinski, Cristian Sarpe, Matthias Wollenhaupt, Tiberio A Ezquerra, Thomas Baumert, and Javier Solis. Nanofabrication of tailored surface structures in dielectrics using temporally shaped femtosecond-laser pulses. *ACS applied materials & interfaces*, 7(12):6613–6619, 2015.
30. B. Rethfeld, K. Sokolowski-Tinten, D. von der Linde, and S.I. Anisimov. Timescales in the response of materials to femtosecond laser excitation. *Applied Physics A*, 79(4):767–769, Sep 2004.
31. B. Rethfeld. Unified model for the free-electron avalanche in laser-irradiated dielectrics. *Phys. Rev. Lett.*, 92:187401, May 2004.
32. Wilbur J Reichman, Denise M Krol, Lawrence Shah, Fumiyo Yoshino, Alan Arai, Shane M Eaton, and Peter R Herman. A spectroscopic comparison of femtosecond-laser-modified fused silica using kilohertz and megahertz laser systems. *Journal of Applied Physics*, 99(12):123112, 2006.
33. James W Chan, Thomas Huser, Joseph S Hayden, Subhash H Risbud, and Denise M Krol. Fluorescence spectroscopy of color centers generated in phosphate glasses after exposure to femtosecond laser pulses. *Journal of the American Ceramic Society*, 85(5):1037–1040, 2002.
34. Richard K Brow, David R Tallant, Sharon T Myers, and Carol C Phifer. The short-range structure of zinc polyphosphate glass. *Journal of Non-Crystalline Solids*, 191(1-2):45–55, 1995.
35. Richard K Brow. Nature of alumina in phosphate glass: I, properties of sodium aluminophosphate glass. *Journal of the American Ceramic Society*, 76(4):913–918, 1993.
36. KO Hill, Y Fujii, Derwyn C Johnson, and BS Kawasaki. Photosensitivity in optical fiber waveguides: Application to reflection filter fabrication. *Applied physics letters*, 32(10):647–649, 1978.
37. Oleg M Efimov, Leonid B Glebov, Larissa N Glebova, Kathleen C Richardson, and Vadim I Smirnov. High-efficiency bragg gratings in photothermorefractive glass. *Applied Optics*, 38(4):619–627, 1999.

1. Introduction

The use of ultrashort laser sources for a variety of scientific, medical and technological applications is continuously increasing [1–3]. In particular femtosecond laser micromachining inside transparent materials has attracted much attention over the last decades [4–17]. Both pulse shaping and spatial beam shaping are currently broadly investigated in order to improve, control and achieve a better understanding of ultrafast laser materials processing [18–20]. For the fabrication of active devices, phosphate glasses are ideal host materials because they can incorporate high concentrations of rare-earth ions. However, many commercially available phosphate glasses exhibit negative index changes under typical laser waveguide writing conditions [21].

We have recently found that fs-laser writing in binary zinc polyphosphate glasses yields good quality waveguides for compositions with [O]/[P] ratios close to 3.25 [22–25]. For practical applications multicomponent glasses offer more robust stability as well as better corrosion resistance. In order to determine if an [O]/[P] ratio of 3.25 is also required in such glasses we investigate femtosecond laser waveguide fabrication in a series of zinc aluminium and zinc magnesium phosphate glasses with [O]/[P] ratios varying between 3.00 and 3.50. We first study the effect of the content of alumina in ternary glasses. We also test the influence of the pulse duration. In this way, we reduce undesired non-linear effects during laser processing as well as premature laser damage. Zinc magnesium phosphate glasses doped with rare earth ions are shown to be suitable for fs-laser fabrication of filters and mirrors by inscribing waveguide Bragg gratings. Finally, we discuss the fs-laser induced structural changes by using Raman confocal spectroscopy.

2. Experimental Methods

2.1. Waveguide writing and characterization

In this work, we use a femtosecond laser amplifier (Merlin-Spitfire LCX, Spectra Physics) that generates a 1 kHz train of Fourier limited pulses of ≈200 fs pulse duration at a wavelength of 800 nm. The pulse duration can be stretched by adjusting the compression stage of the amplifier and characterized using a single shot autocorrelator (SSA Spetra Physics). Figure 1 shows a schematic of the experimental setup employed to inscribe optical waveguides, tracks of modified material and waveguide Bragg gratings inside our set of ternary phosphate glass samples. We control the laser energy delivered inside the sample by using a lambda half wave-plate combined with a polarizing beam cube. Once the energy per pulse is reduced to be equal or less than 10 μJ, we use a confocal system to clean the spatial profile of the laser, which uses two lenses with a f = 500 mm and a pinhole with a diameter of 150 μm. After that, the laser beam is focused inside the glass sample by employing a long working distance microscope objective with a numerical aperture of 0.25. The sample is attached to an Aerotech air bearing stage that translates it along the laser propagation axis at a speed of 50 μm/s. In addition the glass sample is sitting on a 5D holder that allows us to control its precise position along three orthogonal axes and two relevant angles, which are particularly sensitive for measuring the waveguide operation. We monitor the waveguide fabrication using an in situ microscope, that also serves to inspect the input cross section and the lateral view of the inscribed lines. After laser processing, we use a continuous wave laser (660 nm) to check waveguiding operation by measuring the far and near field output modes. We couple the beam into the input facet of the waveguides and image their output end using another lens objective (NA= 0.22, 10x) and an imaging system (tube lens and CCD camera). We additionally measure the numerical aperture of the far field output cone in order to characterize the laser-induced refractive index change.

Waveguide Bragg-grating inscription was carried out using the same experimental setup with a Nikon 50x/0.55 microscope objective (CFI 60 LU PLAN). We translate the sample transversely with respect to the laser beam propagation axis at different processing speeds in order to control the grating index periodicity. We make use of a 400 μm slit to create circular modifications at a writing depth of 250 μm [26, 27]. After laser processing the sample front and back surfaces were ground and polished in order to place the waveguides at the surface for better coupling results. The length of the waveguides after polishing the sample was measured to be 4 mm.

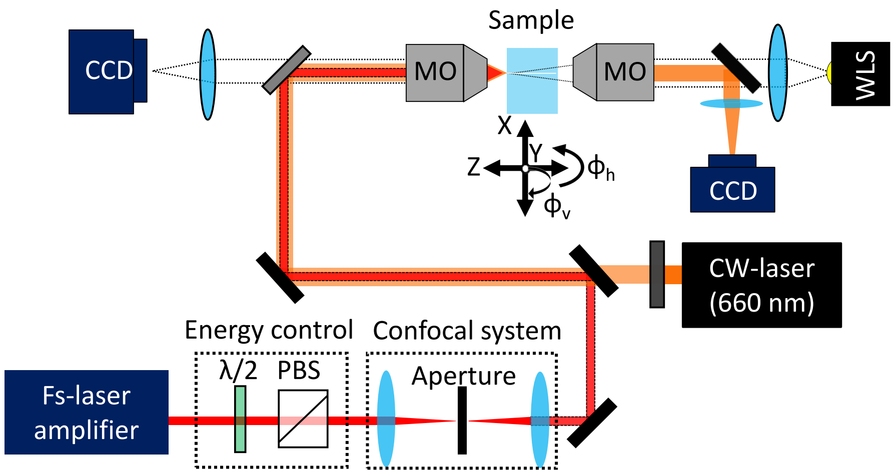

Fig. 1. Experimental setup for waveguide writing, frontal and lateral optical microscopy inspection and near field characterization.

Table 1. Zinc Alumina phosphate glass sample compositions (mole %), [O]/[P] ratios and waveguide operation. These samples are used to study optical waveguiding suitability.

Composition				
ZnO	P_2O_5	Al_2O_3	[O]/[P] ratio	Waveguiding
50	50	0	3.00	No
40	55	5	3.00	No
30	60	10	3.00	No
40	50	10	3.20	No
60	40	0	3.25	Yes
51	44	5	3.25	Yes
42	48	10	3.25	Yes
45	45	10	3.33	No
65	35	0	3.43	No
50	40	10	3.50	No

2.2. Glass sample preparation

We study fs-laser direct-writing inside zinc aluminum phosphate glasses with ten compositions. The glass specimens were prepared by mixing reagent grade Al_2O_3, ZnO, and $NH_4H_2PO_4$ that were calcined at 500 °C for 12 hours in alumina crucibles. Afterwards, they were melted at 1100 °C for 2 hours and subsequently quenched to form a glass frit. The glass was ground with a mortar and remelted in a platinum crucible for 1 hour at 1100 °C. The melts were then poured in steel molds, cooled and annealed near the glass transition temperature. An additional glass sample including magnesium and rare earths was prepared following the same procedure, but employing reagent grade ZnO, MgO, Er_2O_3, Yb_2O_3 and $NH_4H_2PO_4$ in the raw mixture.

We polished the surface of the samples to a flatness better than a $\lambda/5$. The overall surface flatness was characterized using a Zygo interferometer. The samples presented excellent optical quality, with no bubbles or striations, making them ideal for waveguide inscription. Finally, we cleaned the samples before and after fs-laser processing by using organic solvents.

To characterize the precise composition of the glasses, we used energy dispersive spectroscopy (EDS) within a scanning electron microscope (SEM, Helios NanoLab 600), obtaining compositions that are well within the expected tolerances. The levels of ZnO, P_2O_5 and alumina, along with the [O]/[P] ratio of each sample are specified in Table 1. The Er-Yb doped zinc magnesium phosphate glass sample composition is 28 % MgO, 28 % ZnO, 42 % P_2O_5, 1.3 % Yb_2O_3 and 0.7 % Er_2O_3 (mole %). We observe that the SEM data indicate slight discrepancies in the concentration of alumina when compared to the initial raw mixtures, which is likely due to the use of alumina crucibles, and this amount of alumina into the glass is to be expected.

3. Results

3.1. Femtosecond laser waveguide writing in Zinc Aluminum Phosphate glasses

Using our experimental setup we inscribed a variety of tracks of modified material inside glass samples with several compositions (Table 1). A set of laser-induced modifications were systematically made with pulse energies ranging from 0.25 μJ to 10.00 μJ and two different pulse durations (200 fs and 400 fs). We observe three different outcomes, namely unmodified material when using sub-threshold laser energies ($E < E^s_{th}$), tracks with smooth optical changes ($E^s_{th} \leq E < E^d_{th}$) and tracks of damaged material when using higher energies ($E \geq E^d_{th}$). We illustrate the last two in figure 2, where white light microscopy images show the input facet and lateral view of lines inscribed inside the glass sample with a 5 % Al_2O_3, 51 % ZnO and 44 % P_2O_5 composition. They present bright and dark round regions of laser modified material and lateral views that show a smooth (left) and heterogeneous (center) appearance. Microscopy images that present a bright spot are usually good candidates for waveguiding operation. That, we confirm by measuring the near field profile of the guided light using a CW-laser at 660 nm, as shown within the inset on the leftmost image. The one in the center was checked not to guide light. The image on the right illustrates two parallel tracks of damaged material that cannot guide light individually but when machined next to each other they result in a waveguide (see near field profile), where guiding takes place in the region between the damage tracks. However, not every zinc aluminum phosphate glass composition is suitable to be processed and simultaneously result in smooth optical modifications and waveguiding operation. Thus, we explore the suitability of the set of samples presented in Table 1 that contain different alumina levels and [O]/[P] ratios.

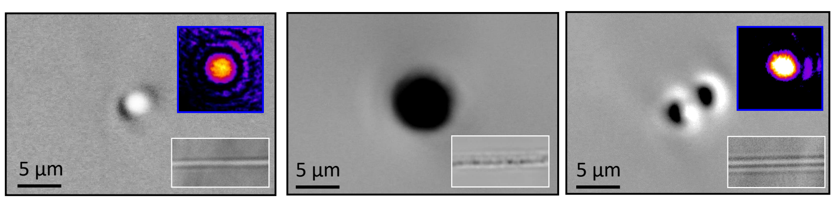

Fig. 2. White light microscopy images of the cross section of a fs-laser machined waveguide (left) and a track of damaged material (center) produced in the sample with a composition of a 5 % Al_2O_3, 51 % ZnO and 44 % P_2O_5. Two parallel adjacent tracks of damage (right) are also shown to guide light in the glass sample with a 60 % ZnO and 40 % P_2O_5. The insets show WLM images of the lateral view and the near field profiles of the waveguides at 660 nm. Note that the image size and grey-scale are the same for all the images.

Figure 3 shows white light microscopy images of lines inscribed inside glass samples with relevant [O]/[P] ratios, (a) 3.00, (b),(c) 3.25 and (d) 3.50 and different alumina contents. We used the same processing conditions to fabricate these lines, *i.e.* 0.5 μJ, 1 kHz and 50 μm/s. The lower row illustrates the near field profiles of the guided modes at 660 nm. We empirically find that zinc aluminium phosphate glass compositions with an [O]/[P] ratio of 3.25 are confirmed to be suitable candidates for waveguide inscription. The micrographs and near field profiles illustrate that waveguiding is not achieved in glasses with [O]/[P]ratios between 3.00≤[O]/[P]<3.25 and

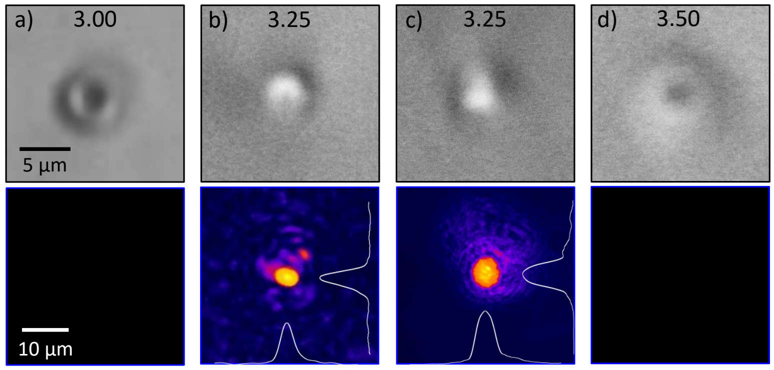

Fig. 3. The top row shows white light microscopy images of the cross section of fs-laser machined lines within glass samples with compositions (a) 30 % ZnO 60 % P_2O_5 10 % Al_2O_3 (b) 42 % ZnO 48 % P_2O_5 10 % Al_2O_3 (c) 51 % ZnO 44 % P_2O_5 5 % Al_2O_3 and (d) 50 % ZnO and 40 % P_2O_5 10 % Al_2O_3. The [O]/[P] ratio is specified on the WLM images. The lower row shows the near field profiles measured for each line using a CW laser at 660 nm. The laser processing conditions were set the same for the four glass compositions, namely a pulse energy of 0.5 μJ, a repetition rate of 1 kHz and a writing speed of 50 μm/s.

3.25<[O]/[P]≤3.50. Those compositions present a negative change in the refractive index within the fs-laser processed region, thus being unable to guide light. Three of the polyphosphate glasses, with an [O]/[P] ratio equal to 3.25, show a positive change in the refractive index, irrespective of their alumina content. We characterized the laser-induced optical change by measuring the numerical aperture of the waveguide through recording the far field profile at a given distance, resulting in δn = $3{\cdot}10^{-4}$. These results are summarized in Table 1 and evidence a clear influence of the glass composition in the suitability for waveguide fabrication, where the ternary phosphate glasses present the same [O]/[P] ratio trend our group reported for binary phosphate glasses [22–25].

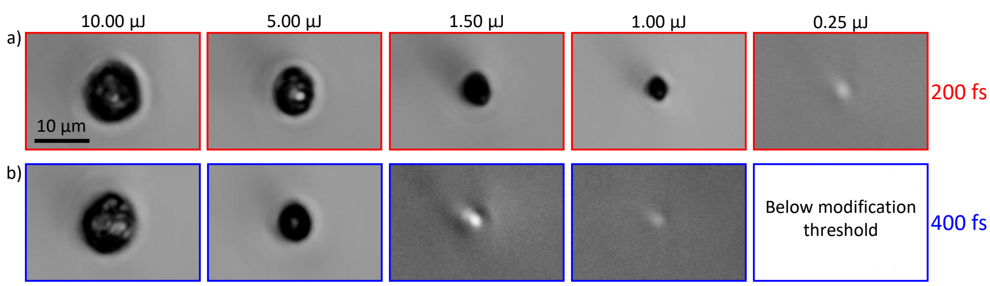

Fig. 4. WLM images of the cross section of fs-laser machined lines of modified glass using a variety of energies and 200 fs (a) and 400 fs (b) laser pulses inside sample 42 % ZnO 48 % P_2O_5 10 % Al_2O_3. The processing speed was kept constant to be 50 μm/s while using a repetition rate of 1 kHz.

In order to reduce undesired non-linear propagation effects and premature laser-induced damage we also tested the fabrication of waveguides using stretched laser pulses. Figure 4 presents white light microscopy images of laser-written lines inside sample 42 % ZnO 48 % P_2O_5 10 % Al_2O_3 (*i.e.* [O]/[P] = 3.25) using several energies (0.25-10.00 μJ) and two pulse durations (a) 200 fs and (b) 400 fs. We observe that the pulse duration has two important effects in the range of laser energies where good waveguides can be produced. First, the energy threshold linked to smooth modifications increases from $E_{th}^{200\,fs}$ = 0.25 μJ to $E_{th}^{400\,fs}$ = 0.50 μJ when using 400 fs laser pulses, see for instance Figure 4 (a) and (b) at 1 μJ. The reason for such threshold increment roots on the inherent non-linearity of the laser energy deposition mechanisms in glasses [28, 29]. In this context, a fs-laser pulse focused inside glass generates a dense electron plasma, whose population rate equations are governed by multiphoton ionization and avalanche ionization, i.e. the former depends on the k^{th} power of the intensity, where $k = \lceil (U_g/\hbar\omega_L) + 1 \rceil$ [30, 31]. The damage threshold is closely related to the number of laser photons used to excite electrons (n_e) as well as to the laser intensity ($dn_e/dt \propto I(t)^k$), which is a measure of the laser energy deposited into the glass. The second observation is an increase of the damage threshold (E_{th}^{d}) or equivalently a simultaneous shift and stretching in the processing regime where good waveguides are obtained $i.e.$ $0.25\ \mu J \ \leq\ E_{200fs}^{wg}\ \leq\ 0.50\ \mu J$ and $0.50\ \mu J \leq\ E_{400fs}^{wg}\ \leq\ 2.50\ \mu J$. This widening on the waveguide fabrication regime facilitates the experiment to further test the validity of glass compositions. We also observe such an effect in glasses with other compositions including i) 60 % ZnO 40 % P_2O_5 and ii) 51 % ZnO 44 % P_2O_5 5 % Al_2O_3. In this way, we confirm that only compositions that have an [O]/[P] ratio equal to 3.25 are feasible candidates to inscribe good quality waveguides thus finding that the reduction of non-linear effects does not facilitate waveguide inscription in glasses with an [O]/[P] ≠ 3.25. Moreover, as long as the [O]/[P] ratio remains equal to 3.25 the content of alumina does not influence the waveguide inscription process up to a 10 % Al_2O_3.

3.2. Raman spectroscopy characterization

The glass samples were investigated with confocal Raman spectroscopy both before and after laser modification in order to elucidate the induced structural changes. We used an excitation CW laser at 473 nm to scan the cross-section of the input facet of the modifications, recording the individual spectrum for each location by using a lens objective (NA = 0.42, 50x) [21, 32, 33]. Figure 5 shows the bulk Raman spectra from unmodified glass samples with varying levels of alumina and a systematically increasing [O]/[P] ratio. The curves have been normalized to the maximum value of the band centered at 400 cm^{-1} so we can easily compare the relative intensities of representative Raman bands after fs-laser modification ($i.e.$ 702 cm^{-1} and 1209 cm^{-1}). A description of the structure and properties of zinc aluminophosphate glasses linked with their Raman spectra is given below, references [34, 35] provide further details.

The spectra presented in figure 5 (a) indicate five unique bands that are caused by vibrations associated with the metaphosphate and polyphosphate glass matrix. The structure of the glass matrix can be described as a network of phosphate tetrahedra that are conected together via corner shared oxygen atoms, forming an interconnected network of long $polymer\ like$ phosphate chains [22, 23, 35]. The elementary units are based on phosphate tetrahedra as shown in the cartoons in figure 5 (b), whose oxygen atoms can be non-bridging atoms. These are categorised using $Q^{(i)}$ terminology, where i denotes the number of bridging oxygens per tetrahedron. The broad Raman signal in the low wavenumber region is due to complex internal deformation bending modes of phosphate chains, both in chain PO_2 and O-P-O bending (350 cm^{-1} bending mode of phosphate polyhedra with zinc modifier and 575 cm^{-1} bend mode related to zinc phosphate network or ZnO_4). The bands around 702 cm^{-1} and 940 cm^{-1} present the symmetric and asymmetric stretching modes of bridging oxygen between two $Q^{(2)}$ tetrahedra, $(POP)_{sym}$ and $(POP)_{asym}$, respectively. The band at 1000 cm^{-1} is assigned to the symmetric stretching modes, $(PO_3)_{sym}$, of terminating P-O bonds on tetrahedra that link to one other tetrahedron ($Q^{(1)}$). The intense band near 1209 cm^{-1} comes from the symmetric stretching associated with the O-P-O non-bridging oxygens on $Q^{(2)}$ phosphate tetrahedra, $(PO_2)_{sym}$. The 1300 cm^{-1} peak on the shoulder of the 1209 cm^{-1} band is the asymmetric stretching of O-P-O non-bridging oxygens, $(PO_2)_{asym}$. The spectra measured in the metaphosphate regime ([O]/[P] = 3.0) illustrate glass

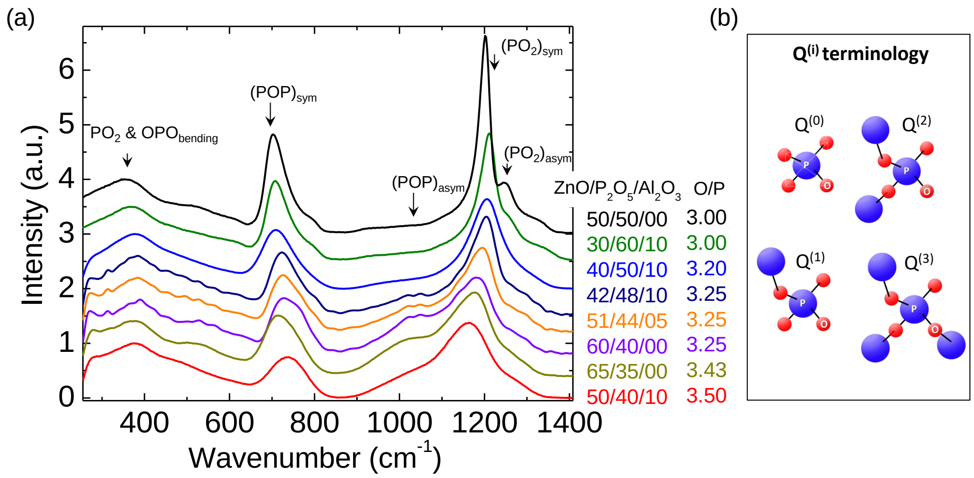

Fig. 5. (a) Raman spectra of the unmodified set of glasses along with composition and [O]/[P] ratios. The main Raman bands and their relation with the vibrational modes are indicated. (b) $Q^{(i)}$ terminology cartoons.

networks based on $Q^{(2)}$ tetrahedra indicating the formation of long metaphosphate chains. As the [O]/[P] ratio increases the Raman spectra reveal that $Q^{(2)}$ tetrahedra, which form long chains in metaphosphate glasses, are substituted by $Q^{(1)}$ tetrahedra. Those $Q^{(1)}$ substitutes terminate shorter chains in the polyphosphate regime ($3.0 < [O]/[P] \leq 3.5$).

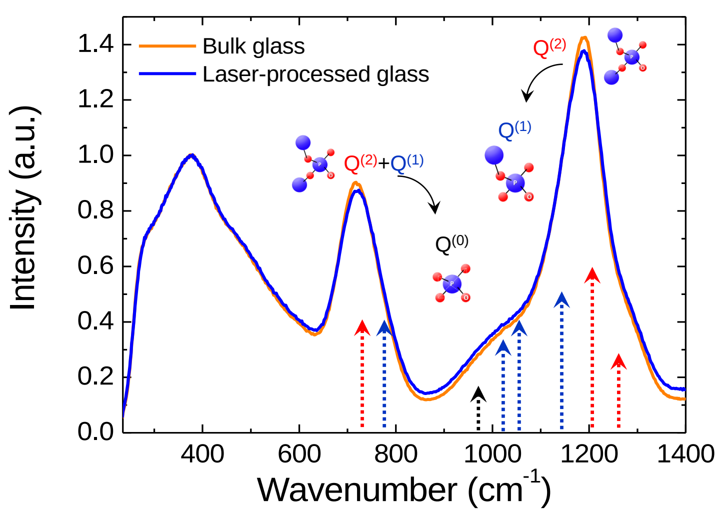

Fig. 6. Raman spectra of unprocessed (orange) and laser-processed (blue) ternary zinc aluminum phosphate glass sample with a 10 % Al_2O_3, 45 % ZnO and 45 % P_2O_5. The arrows show the position for different relevant peaks associated to different vibrational modes, *i.e.* black $Q^{(0)}$, blue $Q^{(1)}$ and red $Q^{(2)}$. The schematics near the Raman bands indicate the depolymerization of $Q^{(2)}$ tetrahedra into $Q^{(1)}$ and $Q^{(0)}$. The track of damage studied here was produced by using a laser pulse energy of 5 μJ, a repetition rate of 1 kHz and a writing speed of 50μm/s.

Figure 6 shows two Raman spectra obtained for laser-modified (blue line) and unmodified (orange line) glass with composition 10 % Al_2O_3, 45 % ZnO and 45 % P_2O_5. The bands centered at 702 cm^{-1} ($(POP)_{sym}$) and 1209 cm^{-1} ($(PO_2)_{sym}$), which are associated to $Q^{(2)}$ tetrahedra, decrease for the laser processed glass. While $Q^{(2)}$ peaks decrease, the Raman bands centered at 1048 cm^{-1} and 970 cm^{-1}, linked to $Q^{(1)}$ and $Q^{(0)}$ tetrahedra, slightly increase. The decrease of $Q^{(2)}$ peaks and increase of $Q^{(1)}$ and $Q^{(0)}$ bands is indicative of a glass depolymerization (*i.e.* $Q^{(2)}$ transforms into $Q^{(1)}$ and $Q^{(0)}$). In addition 1209 cm^{-1} Raman peak also shows a subtle shift towards lower wavenumbers, as previously reported for laser-processed phosphate glasses [22,23].

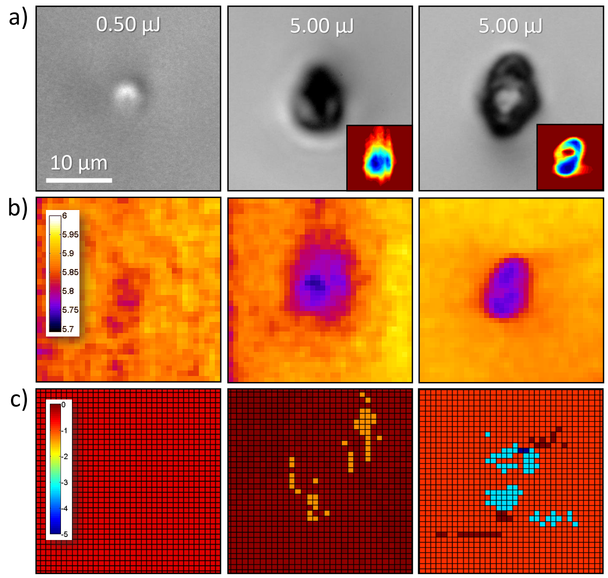

Fig. 7. Optical microscopy (a) and Raman spectral microscopy characterization (b)-(c) of laser fabricated lines inside Zinc Aluminum phosphate glasses. The images in the first and second columns correspond to sample 42 % ZnO 48 % P_2O_5 10 % Al_2O_3 with an [O]/[P] ratio of 3.25, whereas the ones in the third column correspond to sample 45 % ZnO 45 % P_2O_5 10 % Al_2O_3 with an [O]/[P] ratio of 3.33. The false color maps in (b) present the relative amplitude change (a.u.) between 1209 cm^{-1}/1000 cm^{-1} Raman peaks. The false color maps in (c) illustrate the Shift of the 1209 cm^{-1} Raman peak (δcm^{-1}). Note that the whole set of images share the same lateral size. The machined lines studied here were produced by using various laser pulse energies (specified on the optical micrographs), a repetition rate of 1 kHz and a writing speed of 50μm/s.

We have mapped the laser-induced depolymerization for inscribed lines inside two different glasses. Figure 7 shows microscopy images (a) along with Raman maps (b),(c) of tracks inscribed inside glasses with 3.25 (left and center) and 3.33 (right) [O]/[P] ratios. The results in the left column clearly show that there are no significant Raman changes for the sample that shows waveguiding. In contrast, when damage lines are created both the relative Raman intensities and peak positions show changes. These results concur with our earlier work on binary phosphate glasses in that no peak shift was detected even though the glass clearly shows guiding [22] and thus must have undergone a change in index, which is normally associated with a change in the glass network structure. The results on the central and right columns are consistent with an expansion of the glass network and presumably a decrease in the index of refraction thus not allowing for guiding to occur.

3.3. Femtosecond laser-fabricated Bragg gratings

We have so far studied the fabrication of optical waveguides inside binary and ternary zinc aluminum phosphate glasses by testing the role of the glass composition and the laser-induced structural changes. Here, we investigate the use of waveguide Bragg grating (WBG) inscription inside a ternary zinc magnesium phosphate glass (see glass preparation) to create optical filters/mirrors with different spectral characteristics. Typically WBGs are inscribed inside optical fibers to produce fiber Bragg gratings (FBGs) for telecom purposes [36] and also inside bulk material to create volume Bragg gratings (VBGs) [27, 37]. Figure 8 (a) shows a schematic of an optical filter and selective mirror based on a WBG. The cartoon illustrates a periodic refractive index track that forms the Bragg grating. The principle of operation in a WBG roots on the interaction of the light with the periodic refractive index, which selectively reflects and transmits light based on the interference of waves. The condition for light with a particular wavelength to be reflected is $\lambda_{WBG} = 2n_e\Lambda$, where Λ stands for the spatial period of the structure and $n_e = 1.55$ is the refractive index of the glass. Based on this relation, we can precisely design the performance of the laser-fabricated filter by simply calculating the writing speed that will result in a certain spatial period Λ, *i.e.* writing speed = Λ x repetition rate.

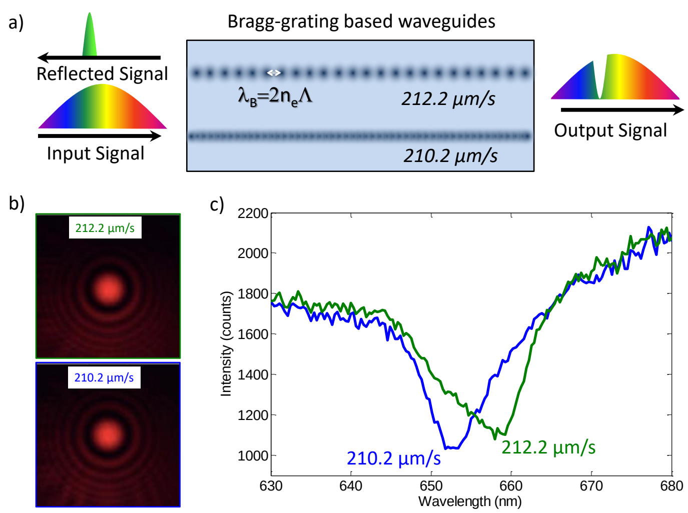

Fig. 8. (a) Waveguide Bragg grating schematic. (b) Near field profiles of WBGs inscribed using two processing speeds inside glass sample with composition 28 % ZnO, 28 % MgO, 42 % P_2O_5, 1.3 % Yb_2O_3 and 0.7 % Yb_2O_3. (c) Transmission spectra of the laser-fabricated WBGs filters.

During fs-laser direct-write, we then control the spatial periodicity of the filter by tuning the processing speed while maintaining the repetition rate (1 kHz) and laser energy (600 nJ). In this way, we write two WBGs using a single pass procedure and two slightly different speeds, *i.e.* 210.2 μm/s and 212.2 μm/s, corresponding to λ_{WBG} = 652 and 658 nm, respectively. Figure 8 (b) shows the near field profiles measured using a CW laser at 660 nm, thus confirming we successfully inscribed the waveguides. The far field numerical aperture was also measured, providing an estimate of the refractive index change of $\approx 10^{-4}$.

Then, we determine the spectral features of the waveguide Bragg gratings by measuring the relative transmission using a white light source (Ocean Optics, DH-2000). We use an optical fiber (Ocean Optics, P100-2 VIS/NIR) to couple the light directly to the input of the waveguides and collect the transmitted light using another fiber (Ocean Optics, P8-2-SMA). Both fibers and the sample are carefully aligned and positioned using micrometer driven translation stages and immersion oil (Cargille Type-B). Figure 8 (c) depicts the transmitted spectra through the WBG. The dips in transmission are centered at 652 nm and 658 nm, respectively for the 210.2 μm/s and 212.2 μm/s processing speeds, in excellent agreement with the predicted values.

Funding

This material is based upon work supported by the National Science Foundation under Grant No. DMR 1206979.

Acknowledgments

We acknowledge fruitful discussions with Luke Fletcher and Charmayne Smith. We are also grateful to Vladimir Semenov and Nikolay Skovorodnikov for support with the laser experiments. We thank Gordon Soekland for assistance on grinding and polishing procedures.

4. Conclusion

In this work we studied the suitability of ternary phosphate glasses for femtosecond laser micromachining of a variety of devices. We tested ten zinc aluminium phosphate glasses with increasing [O]/[P] ratios for fabricating optical waveguides and an Er/Yb doped zinc magnesium phosphate glass for inscribing waveguides Bragg gratings using fs-laser pulses. We were able to produce optical waveguides inside zinc aluminium phosphate glasses with an [O]/[P] ratio equal to 3.25 independently of the aluminium content, resulting in a refractive index change of $3{\cdot}10^{-4}$. We found that longer pulse durations lead to a widening in the range of processing energies that result in waveguiding operation. Using confocal Raman spectroscopy we correlated femtosecond laser-induced damage to an apparent depolymerization of the glass network, where $Q^{(2)}$ species decrease while $Q^{(1)}$ and $Q^{(0)}$ increase. Finally we illustrate the fs-laser fabrication and design of filters and mirrors inside a ternary zinc magnesium phosphate glass with selective spectral features based on waveguide Bragg gratings.